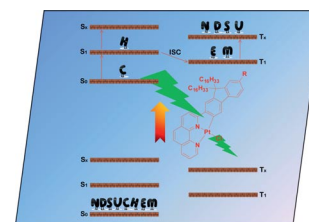


DOI:10.1002/ejic.201300466

Platinum(II) Complexes Bearing 2-(9,9-Dihexadecyl-7-R-fluoren-2-yl)-1,10-phenanthroline Ligands: Synthesis, Photophysics and Reverse Saturable Absorption

Xu-Guang Liu^[a] and Wenfang Sun*^[a]



COVER PICTURE

Keywords: Platinum / Ligand design / Electronic structure / Time-resolved spectroscopy / Emission / Absorption

Six platinum(II) complexes bearing 2-(9,9-dihexadecyl-7-R-fluoren-2-yl)-1,10-phenanthroline ligands (R = NO₂, CN, I, H, benzothiazole, thiophene for ligands **1–6**, respectively) were synthesized and their photophysics and reverse saturable absorption (RSA) were systematically investigated. All complexes exhibit intense absorption bands between 350 and 450 nm, which are attributed to ¹π,π*/¹ILCT (intraligand charge transfer) transitions, and broad ¹MLCT (metal to ligand charge transfer) transitions between 475 and 550 nm. All complexes are emissive at room temperature in a variety of solvents and at 77 K in butyronitrile glassy matrix, with the long-lived, structured emission appearing between 600 and 750 nm. The emitting states are assigned to predominantly the ³π,π* state with an admixture of ³MLCT characters. Upon ns laser excitation at 355 nm, all complexes display broad,

moderately strong transient absorption from the visible to the near-IR region. As a result, RSA is observed from all complexes at 532 nm for ns laser pulses. The strength of the RSA for these complexes follows the trend: Pt-2 > Pt-3 > Pt-4 > Pt-1 >> Pt-5 > Pt-6, which correlates well with the trend of the estimated $\Phi_T \sigma_{ex} / \sigma_0$ values (where Φ_T is the triplet excited state quantum yield, and σ_{ex} and σ_0 are the excited-state and ground-state absorption cross-section, respectively) at 532 nm. It is revealed that substitution at the 7-position of the fluorenyl component exerts a distinct effect on the photophysics and RSA of the complexes. Aromatic substituents such as benzothiazol-2-yl and 2-thionyl cause pronounced red-shifts of the absorption bands, the emission bands, and the transient difference absorption bands, but a decrease of the RSA at 532 nm.

Introduction

Square-planar platinum(II) terdentate complexes represent an interesting class of transition-metal complexes due to their unique photophysical properties, such as room temperature phosphorescence and broadband excited-state absorption.^[1] In addition, the photophysical properties of the Pt^{II} complexes can be readily tuned through structural modifications to tailor the specific requirements for different applications, such as light-emitting devices,^[2] chemosensors,^[3] chemical cells for hydrogen generation,^[4] solar cells,^[5] and nonlinear optical devices.^[6–9]

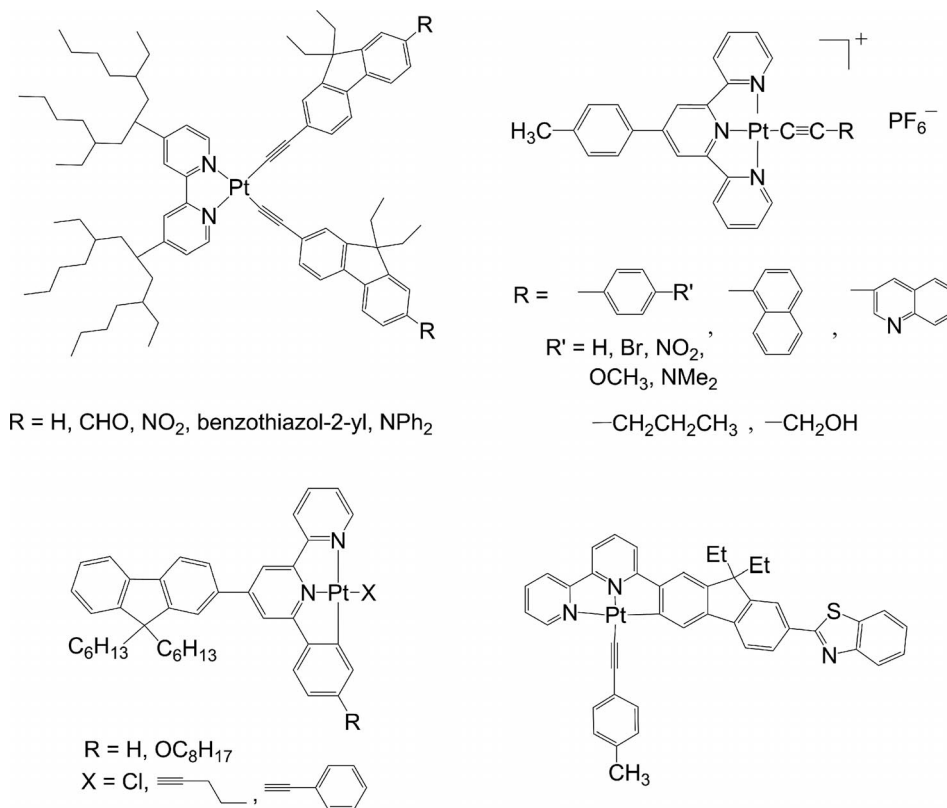
Among the various potential applications, our group is particularly interested in the nonlinear absorption of square-planar platinum complexes. Parallel to the growing interest in the development of phosphane platinum complexes as nonlinear absorbing materials,^[6] there has also been immense interest in the investigation of polypyridine ligands (especially bipyridyl and terpyridyl) for Pt^{II} acet-

ylides.^[6b,7–9] Our group has designed and synthesized several series of Pt^{II} complexes for nonlinear transmission applications, including bipyridyl Pt^{II} acetylide complexes,^[7] terpyridyl Pt^{II} acetylides or chlorides,^[8] and 4,6-diphenyl-2,2'-bipyridyl Pt^{II} acetylides or chlorides.^[9] Some representative structures are shown in Scheme 1. Among these, Pt^{II} complexes bearing 6-phenyl-2,2'-bipyridine ligand (C[^]N[^]N) are particularly interesting because of their relatively intense emission at room temperature compared with the corresponding Pt^{II} terpyridyl complexes.^[10] This feature is attributed to the stronger π-donating ability of the phenyl ring, which admixes the intraligand charge transfer (ILCT) character into the lowest excited state. Meanwhile, the C[^]N[^]N ligand reduces the distortion of the square-planar configuration around the Pt^{II} ion in comparison with the terpyridine ligand, which decreases the nonradiative decay from the excited state. In addition, the Pt(C[^]N[^]N) complexes exhibit broader and stronger nonlinear absorption in the visible to the near-IR region.

Intrigued by the merits of the C[^]N[^]N ligand, we recently replaced the 6-phenyl group at the bipyridine by the 6-(fluoren-2-yl) group (structures shown in Scheme 1) to increase the π-donating ability of the cyclometalated aryl ring and thus enhance the intraligand charge transfer character and nonlinear absorption in the Pt^{II} complex.^[9d] Our photophysical and nonlinear absorption studies revealed

[a] Department of Chemistry and Biochemistry, North Dakota State University, Fargo, ND 58108-6050, USA
Fax: +1-701-231-8831
E-mail: Wenfang.Sun@ndsu.edu
Homepage: <http://www.ndsu.nodak.edu/chemistry/people/faculty/sun.html>

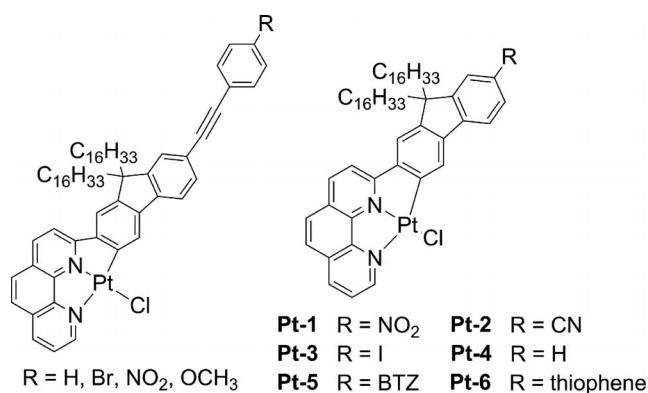
Supporting information for this article is available on the WWW under <http://dx.doi.org/10.1002/ejic.201300466>.



Scheme 1. Representative structures of some bipyridyl Pt^{II} acetylides, terpyridyl Pt^{II} acetylides, and C^NN Pt^{II} acetylides or chlorides.

that the Pt^{II} complex with this new type of C^NN ligand possesses longer triplet excited-state lifetime and broader-band nonlinear absorption in comparison to complexes with the 6-phenyl-2,2'-bipyridine ligand.^[9c,9f] Che and co-workers also discovered that the emission quantum yields of the Pt^{II} C^NN complexes with extended π -conjugation at the lateral rings of the cyclometalating ligands could increase the emission quantum yields.^[11] Encouraged by these results, we recently reported Pt^{II} complexes with a new type of C^NN ligand {2-[9,9-dihexadecyl-7-(4-R-phenylethynyl)-fluoren-2-yl]-1,10-phenanthroline},^[12] in which a rigid 1,10-phenanthroline unit was used to replace the bipyridine unit to favor metal binding (due to the juxtaposed nitrogen atoms held by the rigidity of phenanthroline) and extend the π -conjugation of the ligand (see structures depicted in Scheme 2). In addition, the 4-R-phenylethynyl substituent was introduced at the 7-position of the fluorenyl component to further increase the π -conjugation of the ligand. It is found that all these complexes possess long-lived $^3\pi,\pi^*$ excited states and give rise to moderate emission and broad-band transient absorption. However, the reverse saturable absorption (RSA) of these complexes for nanosecond laser pulse at 532 nm was very weak due to their small ratios of excited-state absorption cross-section relative to that of the ground-state absorption. Furthermore, the auxiliary substituent on the phenylethynyl motif exhibits a negligible effect on the electronic absorption and emission energies of the complexes, indicating that the electron distributions of

the frontier molecular orbitals are essentially localized on the fluorenylphenanthroline components.



Scheme 2. Structures for Pt^{II} chloride complexes containing the 2-[9,9-dihexadecyl-7-(4-R-phenylethynyl)-fluoren-2-yl]-1,10-phenanthroline ligand or the 2-(9,9-dihexadecyl-7-R-fluoren-2-yl)-1,10-phenanthroline ligand (Pt-1-6).

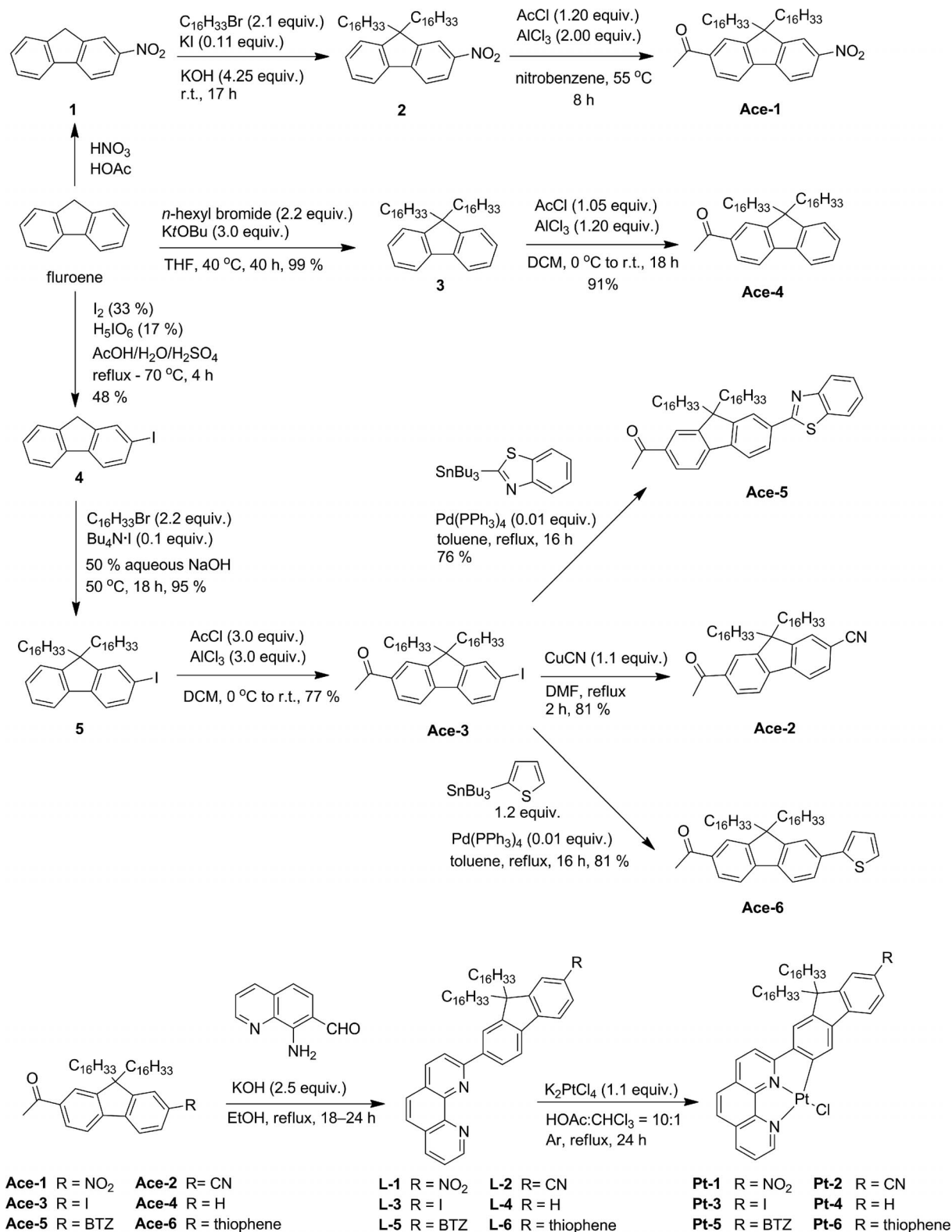
To remedy the deficiency of the Pt^{II} complexes containing the 2-[9,9-dihexadecyl-7-(4-R-phenylethynyl)-fluoren-2-yl]-1,10-phenanthroline ligand, in this work, we designed and synthesized a series of new Pt^{II} 2-(fluoren-2-yl)-1,10-phenanthroline complexes (Pt-1-6) with different substituents directly attached at the 7-position of the fluorene component (structures shown in Scheme 2). Thiophene was chosen as the electron-donating substituent and NO₂, CN,

I, and benzothiazole (BTZ) were chosen as electron-withdrawing substituents. The photophysics of these complexes were systematically investigated with the aim of understanding the structure-property correlations in order to improve the RSA in the Pt^{II} complexes.

Results and Discussion

Synthesis

The synthetic routes to Pt-1–6 are outlined in Scheme 3, and the synthetic details and characterization data for pre-



Scheme 3. Synthetic routes to Pt^{II} complexes Pt-1–6.

cursors Ace-1–6 are provided in the Supporting Information. The synthesis of Ace-3 was previously reported.^[12] Ace-1 was prepared through nitration of fluorene, followed by alkylation of 2-nitrofluorene, and acetylation of the alkylated 2-nitrofluorene using nitrobenzene as solvent.^[13] Ace-2 was synthesized by converting the iodo group in Ace-3 into the corresponding cyano derivative using copper cyanide.^[14] Ace-4 was synthesized by alkylation of fluorene, followed by mono-acetylation of the alkylated fluorene 3.^[11c] Ace-5 and Ace-6 were synthesized by Stille coupling reaction between Ace-3 and the corresponding stannyl compounds.^[15] Ligands L-1–6 were then obtained through the Friedländer condensation reaction between the precursor Ace-1–6 and 8-aminoquinoline-7-carbaldehyde. Finally, the Pt^{II} complexes were synthesized by reacting K₂PtCl₄ with the corresponding ligand under reflux in mixed acetic acid/chloroform (10:1 v/v) solution.

It should be noted that the long alkyl chains were introduced at the 9-position of fluorene to improve the solubility of these cyclometalated Pt^{II} complexes, which is important for the photophysical studies and for future device applications.

Electronic Absorption

The UV/Vis absorption of ligands L-1–6 and Pt^{II} complexes Pt-1–6 was studied in CH₂Cl₂ solutions with different concentrations (1 × 10⁻⁶ to 5 × 10⁻⁴ mol/L). As exemplified in the inset of Figure 1 (b) for Pt-4, the absorption of all ligands and complexes obeys Beer's law in the concentration range studied, indicating the absence of ground-state aggregation in this concentration range. The UV/Vis absorption spectra of L-1–6 and Pt-1–6 are illustrated in Figure 1 and the band maxima and molar extinction coefficients of Pt-1–6 are listed in Table 1. For ligands L-1–6, the intense absorption bands between 300 and 400 nm are dominated by ¹π,π* transitions, whereas the low-energy shoulders have contributions from intraligand charge transfer (¹ILCT) transitions from the electron-donating fluorenyl

component to the electron-withdrawing phenanthrolyl component. The ¹ILCT nature of this shoulder is supported by titration experiments of the ligand with TsOH. As exemplified in the inset of Figure 1 (a) for ligand L-4, the intensity of this shoulder increases and red-shifts with addition of TsOH acid. This feature is attributed to the enhanced electron-withdrawing ability of the phenanthrolyl component after protonation. Substitution at the 7-position of the

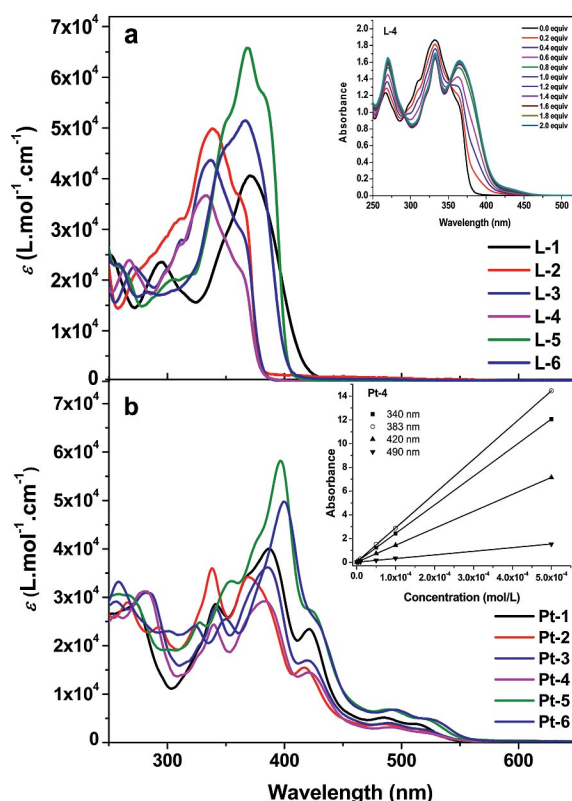


Figure 1. UV/Vis absorption spectra of (a) L-1–6 and (b) Pt-1–6 in CH₂Cl₂. The inset in (a) shows the titration curves of L-4 in CH₂Cl₂ (5 × 10⁻⁵ mol/L) with pTsOH (2 × 10⁻² mol/L). The inset in (b) manifests the Beer's law of Pt-4 in CH₂Cl₂ at different wavelengths.

Table 1. Photophysical parameters for Pt-1–6.

	λ_{abs} [nm] (ϵ [10 ³ L mol ⁻¹ cm ⁻¹])	λ_{em} [nm] (τ_0 [μs]; k_q [× 10 ⁸ L mol ⁻¹ s ⁻¹]) ^[a]	Φ_{em} ^[a]	λ_{em} [nm] (τ_{em} [μs]) ^[b]	$\lambda_{\text{T1-Tn}}$ [nm] (τ_{TA} [μs]; $\epsilon_{\text{T1-Tn}}$ [L mol ⁻¹ cm ⁻¹]) ^[c]	$\Phi_{\text{T}}^{\text{[c]}}$
Pt-1	341 (28.5), 387 (39.8), 421 (23.4), 484 (5.2), 515 (3.8)	618 (3.90; 10.4), 672 (4.02; 8.35)	0.061	607 (5.68), 664 (5.79)	455 (3.48; 35120), 655 (3.65; 39510)	0.34
Pt-2	338 (36.0), 369 (34.2), 416 (15.6), 488 (3.7), 518 (2.3)	612 (5.52; 11.3), 666 (5.35; 11.2)	0.087	600 (7.48), 655 (7.45)	420 (3.49; 44643), 565 (3.63; 49895)	0.38
Pt-3	341 (27.7), 386 (36.0), 421 (16.9), 488 (4.1), 519 (2.9)	614 (7.69; 11.4), 668 (7.97; 11.5)	0.137	598 (11.5), 653 (11.2)	420 (5.36; 37109), 565 (4.93; 65654)	0.18
Pt-4	340 (24.2), 383 (29.1), 421 (14.4), 491 (3.2), 520 (2.1)	614 (8.45; 13.8), 666 (8.60; 13.4)	0.128	598 (12.3), 652 (11.7)	420 (6.47; 39563), 490 (5.57; 55854)	0.21
Pt-5	327 (24.7), 354 (33.2), 397 (58.3), 423 (27.3), 488 (7.1), 523 (4.8)	624 (6.53; 7.13), 676 (6.13; 6.20)	0.079	611 (8.83), 668 (8.73)	465 (4.69; 22901), 640 (4.89; 41441)	0.46
Pt-6	350 (25.4), 400 (49.7), 426 (25.5), 495 (6.8), 526 (5.0)	630 (7.65; 7.90), 678 (6.66; 7.33)	0.062	618 (13.1), 673 (12.7)	465 (5.18; 24144), 655 (4.98; 39234)	0.50

[a] Measured at room temp. at a concentration of 1 × 10⁻⁵ mol/L in CH₂Cl₂ solution. τ_0 is the intrinsic lifetime at infinite dilute concentration, k_q is the self-quenching rate constant. [b] Measured at 77 K at a concentration of 1 × 10⁻⁵ mol/L in BuCN glassy matrix. [c] Measured in toluene.

fluorene component causes red-shifts and enhanced molar extinction coefficients of the ligand. This becomes more salient in **L-1**, **L-5**, and **L-6**, which contain the strong electron-withdrawing NO₂ substituent, the aromatic BTZ, or thiophene substituents, respectively.

The ligand-based ¹π,π* transition bands between 350 and 400 nm are red-shifted in complexes **Pt-1–6** compared with those of their respective ligands, implying the interactions of the ligand-centered molecular orbitals with the platinum dπ orbitals, which result in delocalization of the molecular orbitals and red-shifted absorption bands. The ¹ILCT bands at 420–430 nm in these complexes become more distinct and red-shifted in comparison with those in their ligands, reflecting the increased electron-deficiency of the phenanthrolyl component after complexation with the Pt^{II} ion. Similar spectral features and assignments have been reported by Che's group and our groups for Pt^{II} complexes containing the fluorene unit.^[11c,12] In contrast to the ligands, all complexes possess two broad, moderately intense absorption bands in the visible spectral region, i.e., 470–560 nm, which likely arise from metal-to-ligand charge transfer (¹MLCT) transitions. The appearance of two distinct bands in this region indicates two orbitally distinct MLCT transitions due to unequal interaction of the ligand field with the participating Pt^{II} d-orbitals of different symmetry. A similar feature has been reported by Schanze's group for diimine Pt^{II} bis-acetylide complexes^[16] and by our group for Pt^{II} terpyridyl acetylide complexes^[8b] and for Pt^{II} complexes with a similar type of C[^]N[^]N[^] ligand.^[12] The charge transfer nature of the low-energy absorption bands is supported by the negative solvatochromic effects (i.e., the absorption bands hypsochromically shift in polar solvents such as CH₃CN and CH₂Cl₂, but bathochromically shift in less polar solvents such as hexane and toluene, as exemplified in Figure 2 for **Pt-3** and in Figure S3 of the Supporting Information for **Pt-1**, **Pt-2**, and **Pt-4–6**), which is commonly seen in many Pt^{II} C[^]N[^]N[^] complexes^[9a,9e,9f] and in Pt^{II} terpyridyl complexes.^[8b]

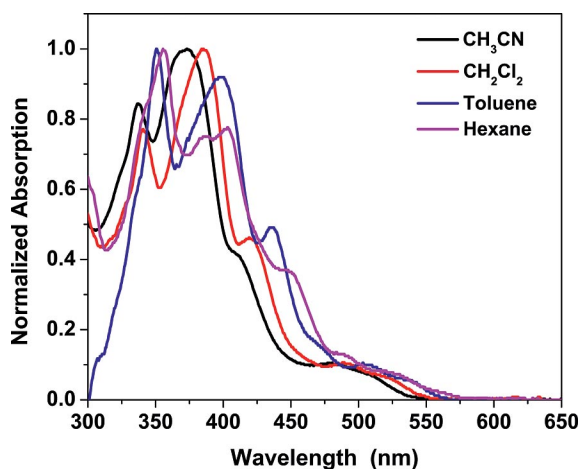


Figure 2. Normalized UV/Vis absorption spectra of **Pt-3** in different solvents.

It is noted that the auxiliary substituent at the 7-position of the fluorene motif exhibits a pronounced effect on the UV/Vis absorption of the Pt^{II} complexes. Similar to that observed in the ligands, substitution at the 7-position of the fluorene increases the molar extinction coefficients of the absorption bands in Pt^{II} complexes compared with those of **Pt-4** (which has no substituent at the 7-position). However, the different substituents affect the transition energy in different ways. The absorption bands of complex **Pt-2** with the CN substituent are blue-shifted compared with those of **Pt-4**; whereas the absorption bands in all of the other complexes are red-shifted compared with those of **Pt-4**. The bathochromic shift and enhancement of the molar extinction coefficients are more significant in **Pt-5** and **Pt-6**, which contain conjugated aromatic substituents. It is noted that the molar extinction coefficients of complexes **Pt-5** and **Pt-6** at 532 nm are much larger than those of the other four complexes, which could decrease the reverse saturable absorption (RSA) at 532 nm for these two complexes and will be discussed later.

Emission

All complexes **Pt-1–6** are emissive in solutions at room temperature and in glassy matrix at 77 K. The normalized emission spectra of these complexes in CH₂Cl₂ at a concentration of 1 × 10⁻⁵ mol/L are illustrated in Figure 3. The emission lifetimes and quantum yields are summarized in Table 1.

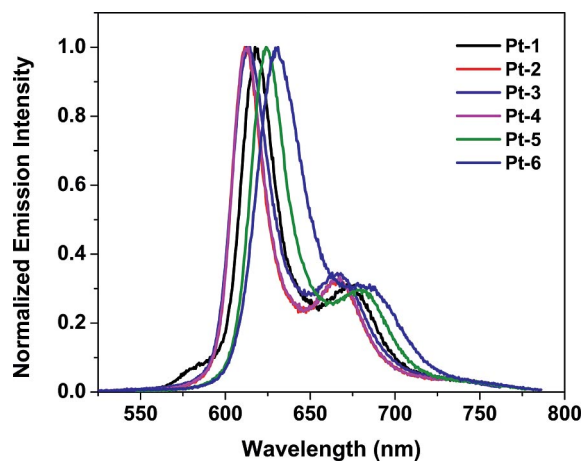


Figure 3. Normalized emission spectra of complexes **Pt-1–6** in CH₂Cl₂ at room temperature (*c* = 1 × 10⁻⁵ mol/L). λ_{ex} = 386 nm for **Pt-1**; 370 nm for **Pt-2**; 386 nm for **Pt-3**; 370 nm for **Pt-4**; 396 nm for **Pt-5**; and 398 nm for **Pt-6**.

As shown in Figure 3, upon excitation of CH₂Cl₂ solutions of **Pt-1–6** at their respective major ¹π,π* absorption bands, a structured emission appears at 612–630 nm and a shoulder at 666–678 nm. The vibronic progressions are 1300 cm⁻¹ for **Pt-1**, 1188 cm⁻¹ for **Pt-2**, 1317 cm⁻¹ for **Pt-3**, 1271 cm⁻¹ for **Pt-4**, 1233 cm⁻¹ for **Pt-5**, and 1124 cm⁻¹ for **Pt-6**, which all fall in the ring breathing mode of the aromatic rings. The lifetimes of the emission vary from approximately 4.0 to 8.5 μs. Considering the large Stokes shifts

(2950–3240 cm^{-1}), the long lifetimes, and the distinct vibronic structures, we attribute the emission of Pt-1–6 at room temperature predominantly to $^3\pi,\pi^*$ states. However, contributions from the $^3\text{MLCT}$ states should also be taken into account in view of the salient negative solvatochromic effect exemplified in Figure 4 (a) for Pt-4 and in the Supporting Information Figures S4 for the other complexes.

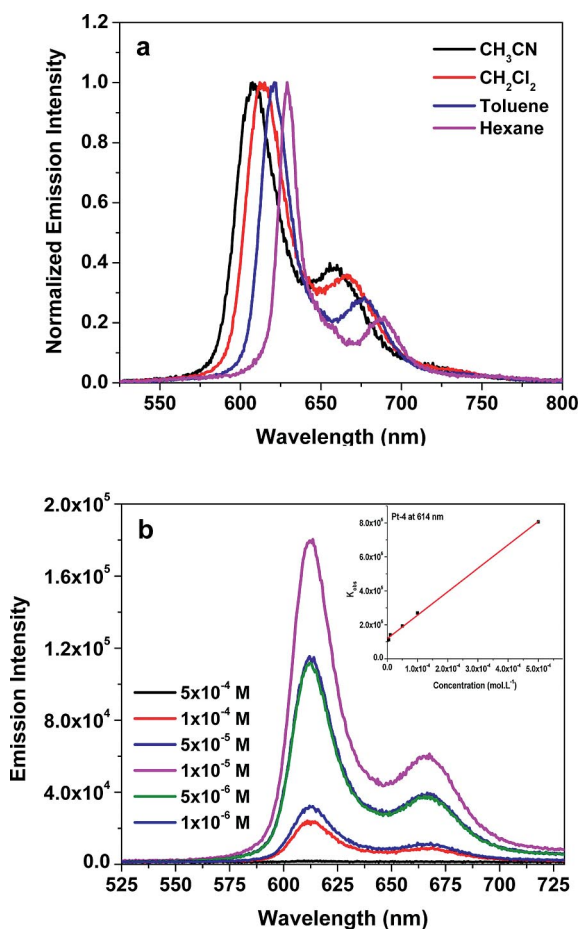


Figure 4. (a) Normalized emission spectra of Pt-4 in different solvents at room temperature ($\lambda_{\text{ex}} = 436 \text{ nm}$). (b) Concentration-dependent emission spectra of Pt-4 in CH_2Cl_2 at room temperature ($\lambda_{\text{ex}} = 370 \text{ nm}$). The inset shows the Stern–Volmer plot of Pt-4 at 614 nm.

The emission energies of the complexes are influenced by the substituents at the 7-position of the fluorene motif. A strong electron-withdrawing substituent (NO_2) or aromatic substituents (BTZ and thiophene) cause pronounced redshifts of the emission spectra in Pt-1, Pt-5, and Pt-6 in comparison to the spectrum of Pt-4. This trend is consistent with that observed from the UV/Vis absorption spectra. However, weaker electron-withdrawing substituents (CN and I) exhibit only a minor effect on the emission energies of Pt-2 and Pt-3.

The emission of Pt-1–6 in CH_2Cl_2 at different concentrations at room temperature was studied, and the results are exemplified in Figure 4 (b) for complex Pt-4 and in the Supporting Information Figures S5 for the other five complexes. It is clear that the emission intensity increases at low

concentrations (1×10^{-6} – $1 \times 10^{-5} \text{ mol/L}$), and the intensity reaches the maximum at a concentration of $1 \times 10^{-5} \text{ mol/L}$. When the concentration was higher than $1 \times 10^{-5} \text{ mol/L}$, the emission intensity continued to decrease. In contrast, the lifetime becomes shorter with increased concentration from 1×10^{-6} to $5 \times 10^{-4} \text{ mol/L}$. The reduced lifetime at higher concentrations clearly indicates the occurrence of self-quenching, which contributes partially to the reduced emission intensity at higher concentrations. By plotting the observed decay rate constants vs. concentrations, straight lines are generated (exemplified in the inset b of Figure 4 for Pt-4 at 614 nm). According to the Stern–Volmer equation [Equation (1) in the experimental section], the self-quenching rate constant (k_q) can be obtained from the slope of the plot, and the intrinsic lifetime (τ_0) can be deduced from the intercept of the plot. The τ_0 and k_q for Pt-1–6 are listed in Table 1. The k_q values for these complexes are of the order 10^8 – $10^9 \text{ L mol}^{-1} \text{ s}^{-1}$, which are in accordance with the values reported for other C^NN Pt complexes^[9e,12] and for Pt terpyridyl complexes.^[17]

To further understand the nature of the emission from the Pt^{II} complexes, the emission characteristics of the ligands and complexes in butyronitrile matrix at 77 K were investigated. As exemplified in Figure S7 of the Supporting Information for ligand L-4, the emission of all of the ligands at 77 K displays the same energies as those at room temperature but with distinct vibronic structures, which is attributed to low-temperature fluorescence. However, weak phosphorescence from 480 to 600 nm was observed in addition to the fluorescence signal when an excess amount of iodomethane (CH_3I) was added due to enhanced intersystem crossing from the heavy-atom effect. For complexes Pt-1–6, owing to the rigidochromic effect,^[18] the emission spectra at 77 K are narrower and slightly blue-shifted with respect to those at room temperature (shown in Figure S8). The vibronic spacing is approximately 1400 cm^{-1} for all complexes, and the thermally induced Stokes shifts vary from 293 to 436 cm^{-1} for these complexes. These features (the similar shape and vibronic spacing of the spectra at 77 K and at room temperature, and the small thermally induced Stokes shift) suggest that the emission of Pt-1–6 at 77 K should also arise predominantly from the ligand-localized $^3\pi,\pi^*$ state.

Transient Absorption

The nanosecond transient difference absorption (TA) spectra of Pt-1–6 in toluene were studied to understand the spectral features of the triplet excited state and deduce its lifetime. Figure 5 (a) illustrates the TA spectra of Pt-1–6 in degassed toluene solution at zero delay after 355 nm excitation. All complexes exhibit a bleaching band below 450 nm, which is consistent with the position of the $^1\pi,\pi^*/^1\text{ILCT}$ transition bands in their respective UV/Vis absorption spectra. Above 450 nm, broad positive absorption bands are observed. The shapes of the TA spectra are quite similar for Pt-1, Pt-5, and Pt-6, with two distinct absorption

bands in the visible to the near-IR region. In contrast, the TA spectra of Pt-2 and Pt-3 resemble each other, with a narrow absorption band at ca. 425 nm and two other broad absorption bands at approximately 485 and 560 nm. However, the band at 560 nm is more salient in Pt-2 and Pt-3 compared to that of Pt-4. In line with the trend observed from the UV/Vis and emission spectra, the low-energy TA band is significantly red-shifted in Pt-1, Pt-5, and Pt-6, which contain strong electron-withdrawing or aromatic substituents with respect to those in the other three complexes.

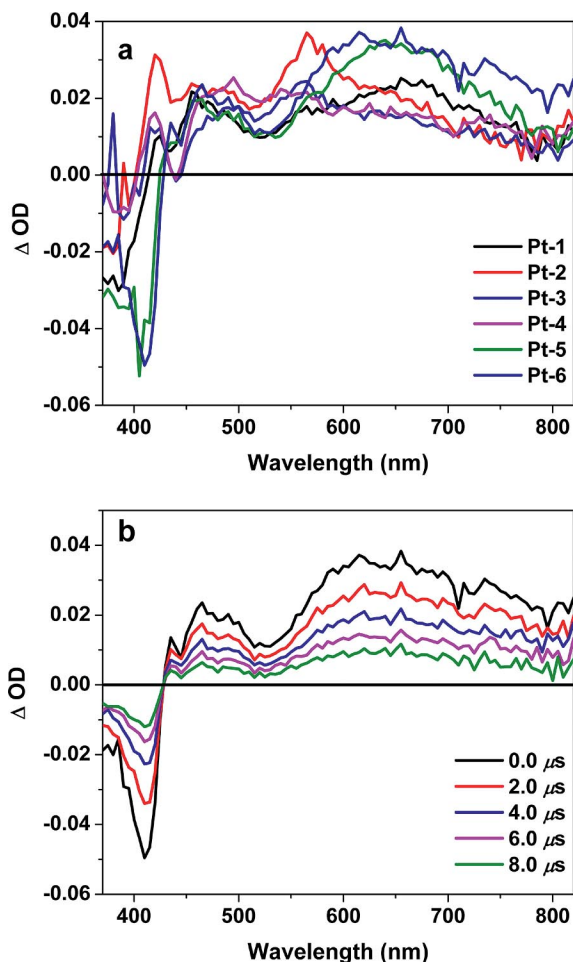


Figure 5. (a) Triplet transient difference absorption spectra of Pt-1–6 at zero time delay following 355 nm excitation in toluene; (b) Time-resolved triplet transient difference absorption spectra of Pt-6 in toluene. For all measurements, $\lambda_{\text{ex}} = 355 \text{ nm}$, $A_{355 \text{ nm}} = 0.4$ in a 1-cm cuvette.

The time-resolved TA spectra are exemplified in Figure 5 (b) for Pt-6 and in Figure S9 of Supporting Information for the other complexes. The TA for all complexes decay monoexponentially throughout the whole spectral range, and the lifetimes deduced from the decay of the TA are in line with those measured from the decay of the emission in the same solution. This feature implies that the TA likely emanates from the same excited state that emits, i.e., predominantly ${}^3\pi,\pi^*$ state possibly mixed with some ${}^3\text{MLCT}$ characters.

Reverse Saturable Absorption (RSA)

RSA is a nonlinear absorption phenomenon in which the excited state of the molecule absorbs stronger than the ground state, resulting in decreased transmission with increased incident energy as illustrated in Figure 6. For an ideal reverse saturable absorber, the molecule should have weak ground-state absorption in order to populate the molecule from the ground state to the excited state through one-photon absorption, and the excited-state absorption should be much stronger than that of the ground state. Namely, the ratio of the excited-state absorption cross-section to that of the ground state ($\sigma_{\text{ex}}/\sigma_{\text{g}}$) should be much larger than 1. Meanwhile, the excited states should be long-lived (at least longer than the laser pulse width), and the triplet excited-state quantum yield should be high in the case of using the triplet excited-state absorption to reach RSA. RSA can be utilized for optical pulse shaping and smoothing, laser pulse compression, and optical switching, etc.^[19] The TA experiments discussed above reveal that complexes Pt-1–6 exhibit stronger excited-state absorption than the ground state and long-lived triplet excited states in the visible to the near-IR region. Consequently, reverse saturable absorption is anticipated to occur in this spectral region. To confirm this notion, nonlinear transmission experiments were conducted for Pt-1–6 using 4.1 ns laser pulses at 532 nm. For easy comparison, the linear transmission of all the complex solutions was adjusted to 80% at 532 nm in a 2-mm cuvette, which guarantees identical excitation of Pt-1–6 to the singlet excited state. The observed different degrees of RSA would then be attributed to the difference in the excited-state absorption, which is related to the excited-state absorption cross-section, lifetime, and quantum yield.

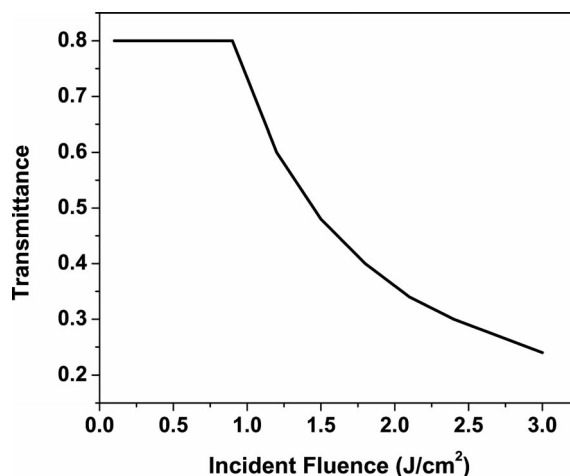


Figure 6. Optical response curve for reverse saturable absorption.

As shown in Figure 7, the transmission of complexes Pt-1–6 decreases drastically when the incident energy increases, which is a clear indication of RSA. The degree of RSA decreases in this order: Pt-2 > Pt-3 > Pt-4 > Pt-1 >> Pt-5 > Pt-6. Complex Pt-2, which contains the CN substituent, displays the strongest RSA; whereas Pt-5 and Pt-6, which

bear aromatic substituents, exhibit the weakest RSA. To rationalize the observed difference in RSA for these complexes, the ratios of the excited-state absorption cross-section relative to that of the ground state ($\sigma_{\text{ex}}/\sigma_{\text{g}}$), which is a critical parameter for RSA, were estimated by following the method described previously.^[20] The resultant ratios are presented in Table 2. According to our previous study on a Pt^{II} complex with similar C[^]N[^]N core structure,^[9d] the excited-state that is the dominant contributor to the RSA of ns laser pulses is the triplet excited state. In such a case, the different triplet excited state quantum yields of these complexes also contribute to the observed RSA. Taking both factors into account, the combined $\Phi_{\text{T}}\sigma_{\text{ex}}/\sigma_0$ values shown in Table 2 roughly correspond to the observed RSA trend for these Pt^{II} complexes. The inconsistency between the $\Phi_{\text{T}}\sigma_{\text{ex}}/\sigma_0$ value and the observed RSA for Pt-1 could possibly be attributed to the different solvents used in our TA and RSA measurements. The TA measurement was performed in toluene (because the Pt^{II} complexes are more stable in toluene than in CH₂Cl₂ upon several hundreds of 355 nm laser irradiation during the TA measurement), but the RSA was measured in CH₂Cl₂ (because of the better solubility of the sample in CH₂Cl₂ than in toluene). It was found that the ground-state absorption cross-section in CH₂Cl₂ is smaller than that in toluene at 532 nm (as implicated in Figure S3 of the Supporting Information), which would increase the $\Phi_{\text{T}}\sigma_{\text{ex}}/\sigma_0$ value in CH₂Cl₂ and result in stronger RSA. Nevertheless, the trend of the estimated $\Phi_{\text{T}}\sigma_{\text{ex}}/\sigma_0$ values are generally in good agreement with the

trend of RSA. It appears that aromatic substitution on this new type of C[^]N[^]N ligand reduces the RSA at 532 nm for Pt-5 and Pt-6. However, considering the reduced ground-state absorption and much stronger excited-state absorption at the longer wavelengths (> 550 nm), it is reasonable to predict that the RSA for these two complexes could be much stronger at wavelengths longer than 550 nm.

Conclusion

The Pt^{II} complexes bearing 2-(9,9-dihexadecyl-7-R-fluorenyl)-1,10-phenanthroline ligands exhibit ¹ π,π^* /¹ILCT transitions below 450 nm and broad ¹MLCT transitions between 475 and 550 nm. Substitution at the 7-position of the fluorenyl component increases the molar extinction coefficients of Pt-1–3, Pt-5 and Pt-6 compared with that of Pt-4, which has no substituent at the 7-position of fluorene. Aromatic substituents (BTZ and thiophene) cause pronounced red-shifts of the absorption bands. All complexes exhibit long-lived, structured ³ $\pi,\pi^*/^3$ MLCT emission at room temperature and at 77 K, with the emission energies being significantly lowered for Pt-5 and Pt-6, which contain aromatic substituents. Upon ns laser excitation at 355 nm, all complexes possess broad, moderately strong transient absorption from the visible to the near-IR region, with the maximum absorption band drastically red-shifted for complexes with strong electron-withdrawing substituent (NO₂) or aromatic substituents (BTZ or thiophene). However, due to the stronger ground-state absorption of these three complexes (Pt-1, Pt-5, and Pt-6) at 532 nm, the $\Phi_{\text{T}}\sigma_{\text{ex}}/\sigma_0$ values for them are smaller than those of the other three complexes. As a result, the RSA of these three complexes (especially the complexes Pt-5 and Pt-6) are weaker than the other complexes at 532 nm. The strength of the RSA for these complexes follows the trend: Pt-2 > Pt-3 > Pt-4 > Pt-1 >> Pt-5 > Pt-6. However, it is believed that the RSA of Pt-1, Pt-5, and Pt-6 could be stronger at longer wavelength in view of the decreased ground-state absorption but increased excited-state absorption in the near-IR region.

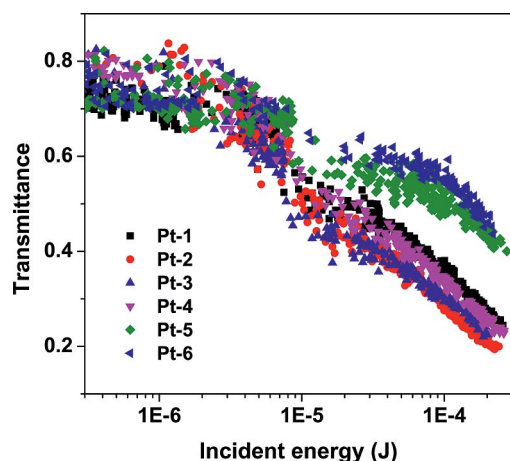


Figure 7. Nonlinear transmission of complexes Pt-1–6 in CH₂Cl₂ solution for 4.1 ns laser pulses at 532 nm. The linear transmission is 80% in a 2-mm cuvette at 532 nm.

Table 2. Ground-state (σ_0) and excited-state (σ_{ex}) absorption cross-sections of the Pt^{II} complexes in toluene at 532 nm.

	Pt-1	Pt-2	Pt-3	Pt-4	Pt-5	Pt-6
σ_0 [10 ⁻¹⁷ cm ²]	1.44	0.95	0.88	0.65	1.77	1.58
σ_{ex} [10 ⁻¹⁷ cm ²]	8.01	11.6	18.3	9.45	11.2	6.10
$\sigma_{\text{ex}}/\sigma_0$	5.57	12.2	20.8	14.5	6.28	3.85
Φ_{T}	0.34	0.38	0.18	0.21	0.46	0.50
$\Phi_{\text{T}}\sigma_{\text{ex}}/\sigma_0$	1.89	4.63	3.74	3.05	2.89	1.93

Experimental Section

Materials and Characterizations: All of the reagents and solvents were purchased from Alfa Aesar or Aldrich Chemical Co., and were used as received unless otherwise stated. The precursor 8-amino-7-quinolinecarbaldehyde was prepared as described previously.^[21] The precursors were characterized by NMR spectroscopic analysis, whereas the final platinum complexes were fully characterized by ¹H NMR, ¹³C NMR, electrospray ionization high-resolution mass spectrometry (ESI-HRMS), and elemental analyses.

NMR spectra were obtained with a Varian Oxford-400 VNMR or a Varian Oxford-500 VNMR spectrometer. ESI-HRMS analyses were conducted with a Bruker Daltonics BioTOF III mass spectrometer. Elemental analyses were carried out by NuMega Resonance Laboratories, Inc., San Diego, California.

The synthetic routes for ligands L-1–6 and Pt^{II} complexes Pt-1–6 are outlined in Scheme 3 and the synthetic details and characterization data are provided below.

Typical Friedländer Condensation^[22] for the Synthesis of Ligands L-1–6: A mixture of 8-aminoquinoline-7-carbaldehyde (1.0 equiv.), Ace-1–6 (1.1 equiv.), and KOH (2.5 equiv.) in absolute EtOH was heated to reflux for 18–24 h under argon and cooled to room temperature. The solvent was evaporated under vacuum and the residue was extracted with ethyl acetate. The organic phase was washed with water three times and dried with anhydrous Na₂SO₄. After removal of the solvent, the residue was purified by column chromatography (neutral Al₂O₃ gel; hexane/ethyl acetate, 10:1–4:1 v/v) to give the pure ligand.

2-(9,9-Dihexadecyl-7-nitro-9H-fluoren-2-yl)-1,10-phenanthroline (L-1): Yield 210 mg (57%); yellow oil. ¹H NMR (400 MHz, CDCl₃): δ = 0.55–0.68 (m, 4 H, CH₂), 0.82 (t, *J* = 7.0 Hz, 6 H, CH₃), 1.00–1.24 (m, 52 H, CH₂), 2.08–2.16 (m, 4 H, CH₂), 7.62 (dd, *J*₁ = 4.4, *J*₂ = 8.0 Hz, 1 H, Ar), 7.75–7.85 (m, 3 H, Ar), 7.92 (d, *J* = 8.0 Hz, 1 H, Ar), 8.12–8.16 (m, 2 H, Ar), 8.20–8.28 (m, 3 H, Ar), 8.32 (d, *J* = 8.4 Hz, 1 H, Ar), 8.46–8.49 (m, 1 H, Ar), 9.21–9.23 (m, 1 H, Ar) ppm; ¹³C NMR (100 MHz, CDCl₃): δ = 14.0, 22.6, 23.8, 29.2, 29.4, 29.5, 29.6, 29.8, 31.9, 40.1, 56.0, 118.2, 120.2, 121.1, 121.6, 122.1, 123.0, 123.3, 126.3, 126.5, 127.6, 128.2, 129.1, 136.1, 136.9, 139.8, 141.0, 146.2, 146.3, 147.2, 147.2, 150.4, 152.5, 152.8, 157.5 ppm; HRMS: *m/z* calcd. for [C₅₇H₇₉N₃O₂ + H]⁺ 838.6245; found 838.6230. C₅₇H₇₉N₃O₂ (838.27): calcd. C 81.67, H 9.50, N 5.01; found C 81.34, H 9.84, N 5.02.

9,9-Dihexadecyl-7-(1,10-phenanthrolin-2-yl)-9H-fluorene-2-carbonitrile (L-2): Yield 140 mg (34%); yellow oil. ¹H NMR (400 MHz, CDCl₃): δ = 0.56–0.65 (m, 4 H, CH₂), 0.83 (t, *J* = 6.8 Hz, 6 H, CH₃), 1.01–1.25 (m, 52 H, CH₂), 2.02–2.11 (m, 4 H, CH₂), 7.61–7.65 (m, 3 H, Ar), 7.76–7.83 (m, 3 H, Ar), 7.89 (d, *J* = 8.0 Hz, 1 H, Ar), 8.11–8.14 (m, 2 H, Ar), 8.25 (d, *J* = 8.0 Hz, 1 H, Ar), 8.33 (d, *J* = 8.4 Hz, 1 H, Ar), 8.45 (d, *J* = 8.0 Hz, 1 H, Ar), 9.21–9.23 (m, 1 H, Ar) ppm; ¹³C NMR (100 MHz, CDCl₃): δ = 14.1, 22.6, 23.8, 29.2, 29.3, 29.5, 29.5, 29.6, 29.9, 31.9, 40.2, 55.8, 110.1, 119.8, 120.6, 121.1, 121.3, 122.0, 123.0, 126.3, 126.5, 127.6, 128.1, 129.1, 131.3, 136.1, 136.9, 140.2, 140.7, 145.3, 146.2, 146.4, 150.4, 151.9, 152.0, 157.6 ppm; HRMS: *m/z* calcd. for [C₅₈H₇₉N₃ + H]⁺ 818.6347; found 818.6358. C₅₈H₇₉N₃·0.5H₂O: calcd. C 84.21, H 9.75, N 5.08; found C 83.95, H 10.02, N 4.93.

2-(9,9-Dihexadecyl-7-iodo-9H-fluoren-2-yl)-1,10-phenanthroline (L-3): Yield 543 mg (59%); yellow oil. ¹H NMR (400 MHz, CDCl₃): δ = 0.66–0.67 (m, 4 H, CH₂), 0.85 (t, *J* = 6.4 Hz, 6 H, CH₃), 1.04–1.29 (m, 52 H, CH₂), 1.96–2.12 (m, 4 H, CH₂), 7.48 (d, *J* = 8.0 Hz, 1 H, Ar), 7.59–7.68 (m, 3 H, Ar), 7.73–7.82 (m, 3 H, Ar), 8.08–8.12 (m, 2 H, Ar), 8.21–8.23 (m, 1 H, Ar), 8.29 (d, *J* = 8.4 Hz, 1 H, Ar), 8.39–8.42 (m, 1 H, Ar), 9.21–9.23 (m, 1 H, Ar) ppm; ¹³C NMR (100 MHz, CDCl₃): δ = 14.1, 22.6, 23.7, 29.2, 29.3, 29.5, 29.6, 29.8, 31.9, 40.3, 55.6, 120.3, 121.0, 121.7, 121.8, 122.8, 126.2, 126.3, 127.4, 127.8, 129.0, 132.1, 135.9, 136.0, 136.7, 139.5, 140.4, 141.3, 146.2, 146.4, 150.4, 150.6, 153.7, 158.0 ppm; HRMS: *m/z* calcd. for [C₅₈H₇₉IN₂ + H]⁺ 919.5361; found 919.5366. C₅₈H₇₉IN₂ (931.18): calcd. C 74.48, H 8.66, N 3.05; found C 74.55, H 8.64, N 3.05.

2-(9,9-Dihexadecyl-9H-fluoren-2-yl)-1,10-phenanthroline (L-4): Yield 260 mg (66%); yellow oil. ¹H NMR (400 MHz, CDCl₃): δ = 0.65–0.72 (m, 4 H, CH₂), 0.84 (t, *J* = 5.6 Hz, 6 H, CH₃), 1.02–1.26 (m, 52 H, CH₂), 1.99–2.10 (m, 4 H, CH₂), 7.28–7.37 (m, 3 H, Ar), 7.58 (dd, *J*₁ = 4.4, *J*₂ = 8.0 Hz, 1 H, Ar), 7.69–7.77 (m, 3 H, Ar), 7.86 (d, *J* = 7.6 Hz, 1 H, Ar), 8.10–8.13 (m, 2 H, Ar), 8.19 (d, *J* = 8.0 Hz, 1 H, Ar), 8.26 (d, *J* = 8.4 Hz, 1 H, Ar), 8.42 (d, *J* = 8.0 Hz,

1 H, Ar), 9.21–9.23 (m, 1 H, Ar) ppm; ¹³C NMR (100 MHz, CDCl₃): δ = 14.0, 22.6, 23.8, 29.24, 29.27, 29.4, 29.5, 29.9, 31.8, 40.4, 55.2, 120.02, 120.06, 129.9, 121.8, 122.73, 122.79, 125.9, 126.2, 126.7, 127.2, 127.3, 127.6, 128.9, 135.8, 136.6, 138.8, 140.6, 142.4, 146.1, 146.4, 150.3, 151.1, 151.3, 158.2 ppm; HRMS: *m/z* calcd. for [C₅₇H₈₀IN₂ + H]⁺ 793.6394; found 793.6406. C₅₇H₈₀IN₂ (920.18): calcd. C 86.30, H 10.17, N 3.53; found C 86.04, H 10.02, N 3.48.

2-[7-(Benzo[d]thiazol-2-yl)-9,9-dihexadecyl-9H-fluoren-2-yl]-1,10-phenanthroline (L-5): Yield 180 mg (59%); yellow solid. ¹H NMR (500 MHz, CDCl₃): δ = 0.69–0.76 (m, 4 H, CH₂), 0.87 (t, *J* = 7.0 Hz, 6 H, CH₃), 1.05–1.29 (m, 52 H, CH₂), 2.17–2.21 (m, 4 H, CH₂), 7.40 (t, *J* = 8.0 Hz, 1 H, Ar), 7.52 (t, *J* = 8.0 Hz, 1 H, Ar), 7.67 (dd, *J*₁ = 4.0, *J*₂ = 8.0 Hz, 1 H, Ar), 7.80 (d, *J* = 9.0 Hz, 1 H, Ar), 7.85 (d, *J* = 9.0 Hz, 1 H, Ar), 7.89 (d, *J* = 8.0 Hz, 1 H, Ar), 7.94 (t, *J* = 8.0 Hz, 2 H, Ar), 8.09–8.14 (m, 2 H, Ar), 8.18–8.20 (m, 3 H, Ar), 8.27–8.29 (m, 1 H, Ar), 8.36 (d, *J* = 8.5 Hz, 1 H, Ar), 8.50 (d, *J* = 7.5 Hz, 1 H, Ar), 9.27 (dd, *J*₁ = 2.0, *J*₂ = 4.5 Hz, 1 H, Ar) ppm; ¹³C NMR (100 MHz, CDCl₃): δ = 14.1, 22.6, 23.8, 29.2, 29.3, 29.53, 29.56, 29.6, 29.9, 31.9, 40.4, 55.7, 120.5, 120.8, 121.1, 121.52, 121.55, 121.9, 122.9, 123.0, 125.0, 126.24, 126.28, 126.3, 127.1, 127.5, 127.9, 129.1, 132.5, 135.0, 136.0, 136.8, 139.7, 141.4, 143.8, 146.2, 146.4, 150.4, 151.9, 152.2, 154.3, 158.0, 168.7 ppm; HRMS: *m/z* calcd. for [C₆₄H₈₃N₃S + H]⁺ 926.6380; found 926.6399. C₆₄H₈₃N₃S (926.44): calcd. C 82.97, H 9.03, N 4.54; found C 83.42, H 9.34, N 4.62.

2-[9,9-Dihexadecyl-7-(thiophen-2-yl)-9H-fluoren-2-yl]-1,10-phenanthroline (L-6): Yield 130 mg (47%); yellow oil. ¹H NMR (400 MHz, CDCl₃): δ = 0.70–0.73 (m, 4 H, CH₂), 0.86 (t, *J* = 6.8 Hz, 6 H, CH₃), 1.05–1.29 (m, 52 H, CH₂), 2.07–2.15 (m, 4 H, CH₂), 7.11 (dd, *J*₁ = 3.6, *J*₂ = 5.2 Hz, 1 H, Ar), 7.25–7.30 (m, 1 H, Ar), 7.39–7.41 (m, 1 H, Ar), 7.60–7.65 (m, 3 H, Ar), 7.77 (d, *J* = 8.4 Hz, 2 H, Ar), 7.82 (d, *J* = 8.8 Hz, 1 H, Ar), 7.87 (d, *J* = 8.0 Hz, 1 H, Ar), 8.14–8.17 (m, 2 H, Ar), 8.24 (dd, *J*₁ = 1.6, *J*₂ = 8.0 Hz, 1 H, Ar), 8.31 (d, *J* = 8.4 Hz, 1 H, Ar), 8.45 (dd, *J*₁ = 1.6, *J*₂ = 8.0 Hz, 1 H, Ar), 9.25 (dd, *J*₁ = 1.6, *J*₂ = 4.4 Hz, 1 H, Ar) ppm; ¹³C NMR (100 MHz, CDCl₃): δ = 14.1, 22.6, 23.8, 29.2, 29.3, 29.5, 29.6, 30.0, 31.9, 40.4, 55.4, 120.2, 120.5, 121.0, 121.9, 122.8, 122.9, 124.5, 124.9, 126.1, 126.4, 127.4, 127.7, 128.0, 129.0, 133.4, 136.0, 136.7, 138.9, 140.3, 141.9, 145.2, 146.2, 146.4, 150.3, 151.3, 152.2, 158.2 ppm; HRMS: *m/z* calcd. for [C₆₁H₈₂N₂S + H]⁺ 875.6271; found 875.6294. C₆₁H₈₂N₂S·toluene (967.5 = 875.39+92.1): calcd. C 84.41, H 9.38, N 2.90; found C 84.62, H 9.51, N 3.42.

Typical Procedures for Complexation with Pt^{II}:^[11c,12] A mixture of L-*x* (1.00 equiv.), [K₂PtCl₄] (1.25 equiv.) in a mixture of chloroform and acetic acid (1:10 v/v) was heated to reflux for 24 h under argon. The orange solid was filtered, washed with water and diethyl ether several times, and then dried.

Complex Pt-1: Yield 106 mg (59%); orange solid. ¹H NMR (400 MHz, CDCl₃): δ = 0.62–0.74 (m, 4 H, CH₂), 0.82 (t, *J* = 6.8 Hz, 6 H, CH₃), 1.04–1.24 (m, 52 H, CH₂), 2.01–2.10 (m, 4 H, CH₂), 7.41 (s, 1 H, Ar), 7.73–7.77 (m, 4 H, Ar), 7.94 (d, *J* = 8.4 Hz, 1 H, Ar), 8.15–8.18 (m, 3 H, Ar), 8.27 (dd, *J*₁ = 1.2, *J*₂ = 8.4 Hz, 1 H, Ar), 8.40 (d, *J* = 8.0 Hz, 1 H, Ar), 9.04 (d, *J* = 4.0 Hz, 1 H, Ar) ppm; ¹³C NMR (100 MHz, CDCl₃): δ = 14.1, 22.7, 23.9, 29.3, 29.5, 29.60, 29.63, 30.0, 31.9, 40.3, 55.4, 118.0, 118.7, 119.6, 121.1, 123.4, 126.1, 126.3, 126.7, 127.0, 127.8, 131.0, 136.5, 137.2, 140.9, 142.2, 146.2, 147.2, 147.4, 148.1, 148.2, 149.4, 152.6, 165.2 ppm; HRMS: *m/z* calcd. for [C₅₇H₇₈ClN₃O₂Pt + Na]⁺ 1089.5323; found 1089.5488. C₅₇H₇₈ClN₃O₂Pt (1067.81): calcd. C 64.12, H 7.36, N 3.94; found C 63.86, H 7.70, N 4.04.

Complex Pt-2: Yield 60 mg (47%); orange solid. ^1H NMR (400 MHz, CDCl_3): $\delta = 0.59\text{--}0.72$ (m, 4 H, CH_2), 0.82 (t, $J = 6.8$ Hz, 6 H, CH_3), 1.04–1.24 (m, 52 H, CH_2), 1.97–2.02 (m, 4 H, CH_2), 7.38 (s, 1 H, Ar), 7.58 (s, 1 H, Ar), 7.64 (d, $J = 8.0$ Hz, 1 H, Ar), 7.72–7.77 (m, 4 H, Ar), 7.91 (d, $J = 8.0$ Hz, 1 H, Ar), 8.11–8.18 (m, 2 H, Ar), 8.39 (d, $J = 8.0$ Hz, 1 H, Ar), 9.04 (d, $J = 4.8$ Hz, 1 H, Ar) ppm; ^{13}C NMR (100 MHz, CDCl_3): $\delta = 14.1, 22.7, 23.9, 29.3, 29.5, 29.60, 29.65, 30.0, 31.9, 40.3, 55.2, 110.3, 118.6, 119.5, 119.9, 121.5, 126.0, 126.2, 126.7, 126.9, 127.5, 131.0, 131.4, 136.4, 137.2, 140.9, 142.7, 145.5, 146.2, 146.8, 147.3, 148.1, 149.4, 152.1, 165.3$ ppm; HRMS: m/z calcd. for $[\text{C}_{58}\text{H}_{78}\text{ClIN}_3\text{Pt} + \text{Na}]^+$ 1069.5429; found 1069.5424. $\text{C}_{58}\text{H}_{78}\text{ClIN}_3\text{Pt}\cdot\text{H}_2\text{O}\cdot\text{Et}_2\text{O}$ (1140.0 = 1047.82+18.0+74.1): calcd. C 65.33, H 7.96, N 3.69; found C 65.42, H 7.73, N 4.20.

Complex Pt-3: Yield 77 mg (39%); orange solid. ^1H NMR (400 MHz, CDCl_3): $\delta = 0.69\text{--}0.84$ (m, 10 H, $\text{CH}_2 + \text{CH}_3$), 1.07–1.25 (m, 52 H, CH_2), 1.93–1.98 (m, 4 H, CH_2), 7.24 (s, 1 H, Ar), 7.50 (d, $J = 8.8$ Hz, 1 H, Ar), 7.53–7.60 (m, 4 H, Ar), 7.66–7.69 (m, 2 H, Ar), 7.89 (s, 1 H, Ar), 7.94 (d, $J = 8.8$ Hz, 1 H, Ar), 8.24 (d, $J = 8.0$ Hz, 1 H, Ar), 8.77 (d, $J = 4.0$ Hz, 1 H, Ar) ppm; ^{13}C NMR (100 MHz, CDCl_3): $\delta = 14.3, 22.9, 24.2, 29.5, 29.6, 29.82, 29.86, 30.3, 32.1, 40.6, 55.2, 93.7, 118.3, 119.6, 122.9, 125.9, 126.1, 126.6, 126.8, 126.9, 131.1, 132.1, 136.2, 136.4, 137.2, 140.8, 141.2, 143.9, 145.6, 145.9, 146.0, 147.7, 149.3, 154.1, 165.3$ ppm; HRMS: m/z calcd. for $[\text{C}_{57}\text{H}_{78}\text{ClIN}_2\text{Pt} + \text{Na}]^+$ 1170.4438; found 1170.4441. $\text{C}_{57}\text{H}_{78}\text{ClIN}_2\text{Pt}$ (1148.70): calcd. C 59.60, H 6.84, N 2.44; found C 59.66, H 7.06, N 2.39.

Complex Pt-4: Yield 44 mg (23%); orange solid. ^1H NMR (400 MHz, CDCl_3): $\delta = 0.67\text{--}0.84$ (m, 10 H, $\text{CH}_2 + \text{CH}_3$), 1.07–1.26 (m, 52 H, CH_2), 1.95–2.05 (m, 4 H, CH_2), 7.28–7.38 (m, 4 H, Ar), 7.52–7.59 (m, 4 H, Ar), 7.85 (d, $J = 6.8$ Hz, 1 H, Ar), 7.96–7.99 (m, 2 H, Ar), 8.26 (d, $J = 8.0$ Hz, 1 H, Ar), 8.82 (d, $J = 4.4$ Hz, 1 H, Ar) ppm; ^{13}C NMR (100 MHz, CDCl_3): $\delta = 14.1, 22.6, 24.1, 29.3, 29.4, 29.60, 29.64, 30.2, 31.9, 40.6, 54.7, 118.0, 119.5, 121.1, 125.5, 125.9, 126.5, 126.8, 126.9, 127.7, 130.9, 136.3, 137.0, 140.9, 141.0, 144.7, 144.9, 145.9, 146.3, 147.4, 149.1, 151.5, 165.4$ ppm; HRMS: m/z calcd. for $[\text{C}_{57}\text{H}_{79}\text{ClIN}_2\text{Pt} + \text{Na}]^+$ 1044.5472; found 1044.5508. $\text{C}_{57}\text{H}_{79}\text{ClIN}_2\text{Pt}$ (1022.81): calcd. C 66.94, H 7.79, N 2.74; found C 67.20, H 8.14, N 2.65.

Complex Pt-5: Yield 110 mg (73%); orange solid. ^1H NMR (400 MHz, CDCl_3): $\delta = 0.62\text{--}0.84$ (m, 10 H, $\text{CH}_2 + \text{CH}_3$), 1.05–1.23 (m, 52 H, CH_2), 2.00–2.14 (m, 4 H, CH_2), 7.35–7.39 (m, 2 H, Ar), 7.49 (t, $J = 7.6$ Hz, 1 H, Ar), 7.67–7.68 (m, 4 H, Ar), 7.89–7.95 (m, 2 H, Ar), 8.04–8.13 (m, 5 H, Ar), 8.34–8.35 (m, 1 H, Ar), 8.98 (d, $J = 3.2$ Hz, 1 H, Ar) ppm; ^{13}C NMR (100 MHz, CDCl_3): $\delta = 14.3, 22.9, 24.2, 29.5, 29.6, 29.8, 30.3, 32.1, 40.7, 55.4, 118.6, 119.8, 121.5, 121.7, 121.8, 123.2, 125.2, 126.0, 126.3, 126.5, 126.9, 127.0, 127.3, 127.5, 131.2, 133.0, 135.3, 136.6, 137.3, 141.0, 144.1, 144.3, 145.9, 146.3, 147.5, 148.1, 149.5, 152.6, 154.5, 165.6, 169.0$ ppm; HRMS: m/z calcd. for $[\text{C}_{64}\text{H}_{82}\text{ClIN}_3\text{PtS} + \text{Na}]^+$ 1177.5458; found 1177.5717. $\text{C}_{64}\text{H}_{82}\text{ClIN}_3\text{PtS}\cdot\text{H}_2\text{O}$: calcd. C 65.48, H 7.21, N 3.58; found C 65.11, H 7.19, N 3.61.

Complex Pt-6: Yield 60 mg (40%); orange solid. ^1H NMR (400 MHz, CDCl_3): $\delta = 0.73\text{--}0.85$ (m, 10 H, $\text{CH}_2 + \text{CH}_3$), 1.12–1.25 (m, 52 H, CH_2), 2.01–2.10 (m, 4 H, CH_2), 7.11 (dd, $J_1 = 3.6, J_2 = 5.2$ Hz, 1 H, Ar), 7.29–7.31 (m, 2 H, Ar), 7.41 (d, $J = 4.0$ Hz, 1 H, Ar), 7.52–7.66 (m, 6 H, Ar), 7.84 (d, $J = 8.0$ Hz, 1 H, Ar), 7.95 (s, 1 H, Ar), 7.98 (d, $J = 8.4$ Hz, 1 H, Ar), 8.27 (d, $J = 8.0$ Hz, 1 H, Ar), 8.83 (d, $J = 4.4$ Hz, 1 H, Ar) ppm; ^{13}C NMR (100 MHz, CDCl_3): $\delta = 14.1, 22.6, 24.1, 29.3, 29.4, 29.6, 30.2, 31.9, 40.6, 54.9, 118.1, 119.5, 119.9, 121.5, 123.0, 124.6, 125.1, 125.5, 125.9, 126.4, 126.5, 126.8, 128.1, 130.9, 133.8, 136.2, 137.0, 140.5, 141.0, 144.4,$

144.8, 145.2, 145.9, 146.5, 147.5, 149.1, 152.4, 165.2 ppm; HRMS: m/z calcd. for $[\text{C}_{61}\text{H}_{81}\text{ClIN}_2\text{PtS} + \text{Na}]^+$ 1126.5349; found 1126.5367. $\text{C}_{61}\text{H}_{81}\text{ClIN}_2\text{PtS}$ (1104.93): calcd. C 66.31, H 7.39, N 2.54; found C 66.16, H 7.33, N 2.62.

Photophysical Measurements: The UV/Vis absorption spectra were acquired with an Agilent 8453 spectrophotometer in HPLC grade solvents. The steady-state emission spectra were recorded with a SPEX fluorolog-3 fluorometer/phosphorometer in different solvents. The emission quantum yields of the Pt^{II} complexes were determined by a comparative method in degassed solutions,^[23] in which a degassed aqueous solution of $[\text{Ru}(\text{bpy})_3]\text{Cl}_2$ ($\Phi_{\text{em}} = 0.042, \lambda_{\text{ex}} = 436$ nm) was used as the reference.^[24] The excited-state lifetimes, the triplet excited-state quantum yields, and the triplet transient difference absorption spectra were measured in degassed solutions with an Edinburgh LP920 laser flash photolysis spectrometer. The third harmonic output (355 nm) of a Nd:YAG laser (Quantel Brilliant, pulsewidth ca. 4.1 ns, repetition rate was set at 1 Hz) was used as the excitation source. Each sample was purged with argon for at least 30 min prior to measurement.

The self-quenching rate constants (k_{q}) in dichloromethane were deduced from the Stern–Volmer equation,

$$k_{\text{obs}} = k_{\text{q}}[c] + k_0 \quad (1)$$

where k_{obs} is the measured radiative decay rate constant of the emission ($k_{\text{obs}} = 1/\tau_{\text{em}}$) at a given concentration, k_{q} is the self-quenching rate constant, $[c]$ is the concentration of the complex in mol/L, and k_0 ($k_0 = 1/\tau_0$) is the decay rate constant of the excited state at infinite dilute solution. A plot of the observed decay rate constant vs. concentration should give a straight line. The slope of the straight line corresponds to k_{q} and the intercept corresponds to k_0 .

The triplet excited-state absorption coefficient (ε_{T}) at the absorption band maximum was measured by the singlet depletion method,^[25] in which the optical density changes during transient absorption at the minimum of the bleaching band (ΔOD_{S}) and the maximum of the positive band (ΔOD_{T}) were recorded; ε_{T} was then calculated using Equation (2)^[25]

$$\varepsilon_{\text{T}} = \frac{\varepsilon_{\text{S}} \times \Delta OD_{\text{T}}}{\Delta OD_{\text{S}}} \quad (2)$$

where ε_{S} is the ground-state molar extinction coefficient at the electronic absorption band maximum.

The quantum yield of the triplet excited state formation (Φ_{T}) was determined by using the comparative method,^[26] in which SiNc in benzene ($\Phi_{\text{T}} = 0.20, \varepsilon_{\text{T},590} = 70,000 \text{ M}^{-1} \text{ cm}^{-1}$)^[27] was used as the reference. All the solutions were optically matched at the excitation wavelength (355 nm), and Φ_{T} was calculated using Equation (3)^[26]

$$\Phi_{\text{T}}^{\text{s}} = \Phi_{\text{T}}^{\text{ref}} \times \frac{\Delta OD_{\text{T}}^{\text{s}}}{\Delta OD_{\text{T}}^{\text{ref}}} \times \frac{\varepsilon_{\text{T}}^{\text{ref}}}{\varepsilon_{\text{T}}^{\text{s}}} \quad (3)$$

where $\Delta OD_{\text{T}}^{\text{s}}$ and $\Delta OD_{\text{T}}^{\text{ref}}$ are the maximum optical density change during transient absorption from the sample and the reference, respectively; $\varepsilon_{\text{T}}^{\text{ref}}$ and $\varepsilon_{\text{T}}^{\text{s}}$ are the triplet molar extinction coefficients of this transition at the wavelength where ΔOD_{T} is measured for the reference and the sample, respectively. $\Phi_{\text{T}}^{\text{ref}}$ is the triplet excited-state quantum yield of the reference.

Nonlinear Transmission Measurements: The experimental setup was similar to a system that has been described previously.^[28] The light source was the second harmonic output ($\lambda = 532$ nm) of a 4.1 ns (fwhm), 10 Hz, Q-switched Quantel Brilliant Nd:YAG laser. $A f =$

30 cm plano-convex lens was used to focus the laser beam to the center of a 2-mm-thick sample cuvette. The radius of the beam waist was ca. 96 μm . Two Molelectron J4-09 pyroelectric probes and an EPM2000 energy/power meter were used to monitor the incident and output energies.

Supporting Information (see footnote on the first page of this article): Details of the synthesis and characterization data for precursors, and additional UV/Vis absorption, emission, and transient difference absorption data and spectra.

Acknowledgments

This work was partially supported by the U.S. National Science Foundation (NSF) (CAREER CHE-0449598) and partially by the Army Research Laboratory (grant numbers W911NF-06-2-0032 and W911NF-10-2-0055).

- [1] a) J. A. G. Williams, *Top. Curr. Chem.* **2007**, *281*, 205–268; b) F. N. Castellano, I. E. Pomestchenko, E. Shikhova, F. Hua, M. L. Muro, N. Rajapakse, *Coord. Chem. Rev.* **2008**, *250*, 1819–1828; c) S. D. Cummings, *Coord. Chem. Rev.* **2009**, *253*, 1495–1516; d) S. D. Cummings, *Coord. Chem. Rev.* **2009**, *253*, 449–478.
- [2] a) J. Kalinowski, V. Fattori, M. Cocchi, J. A. G. Williams, *Coord. Chem. Rev.* **2011**, *255*, 2401–2425; b) J. A. G. Williams, S. Develay, D. L. Rochester, L. Murphy, *Coord. Chem. Rev.* **2008**, *252*, 2596–2611.
- [3] a) K. M. Wong, V. W. Yam, *Coord. Chem. Rev.* **2007**, *251*, 2477–2488; b) V. Guerschais, J. Fillaut, *Coord. Chem. Rev.* **2011**, *255*, 2448–2457; c) Z. Ji, Y. Li, W. Sun, *J. Organomet. Chem.* **2009**, *694*, 4140–4145; d) H. Zhang, B. Zhang, Y. Li, W. Sun, *Inorg. Chem.* **2009**, *48*, 3617–3627; e) K. M. Wong, W. Tang, X. Lu, N. Zhu, V. W. Yam, *Inorg. Chem.* **2005**, *44*, 1492–1498; f) Q. Yang, L. Wu, H. Zhang, B. Chen, Z. Wu, L. Zhang, C. Tung, *Inorg. Chem.* **2004**, *43*, 5195–5197.
- [4] a) K. Sakai, H. Ozawa, *Coord. Chem. Rev.* **2007**, *251*, 2753–2766; b) R. Okazaki, S. Masaoka, K. Sakai, *Dalton Trans.* **2009**, 6127–6133; c) M. Ogawa, G. Ajayakumar, S. Masaoka, H. Kraatz, K. Sakai, *Chem. Eur. J.* **2011**, *17*, 1148–1162; d) S. Masaoka, Y. Mukawa, K. Sakai, *Dalton Trans.* **2010**, *39*, 5868–5876; e) K. Yamauchi, S. Masaoka, K. Sakai, *J. Am. Chem. Soc.* **2009**, *131*, 8404–8406; f) X. Wang, S. Goeb, Z. Ji, N. A. Pogulaichenko, F. N. Castellano, *Inorg. Chem.* **2011**, *50*, 705–707; g) P. Du, J. Schneider, F. Li, W. Zhao, U. Patel, F. N. Castellano, R. Eisenberg, *J. Am. Chem. Soc.* **2008**, *130*, 5056–5058; h) P. Jarosz, P. Du, J. Schneider, S. Lee, D. McCamant, R. Eisenberg, *Inorg. Chem.* **2009**, *48*, 9653–9663.
- [5] a) S. Chakraborty, T. J. Wadas, H. Hester, R. Schmehl, R. Eisenberg, *Inorg. Chem.* **2005**, *44*, 6865–6878; b) E. C. Kwok, M. Chan, K. M. Wong, W. H. Lam, V. W. Yam, *Chem. Eur. J.* **2010**, *16*, 12244–12254; c) W. Wong, C. Ho, *Acc. Chem. Res.* **2010**, *43*, 1246–1256.
- [6] a) C. Liao, A. H. Shelton, K. Kim, K. S. Schanze, *ACS Appl. Mater. Interfaces* **2011**, *3*, 3225–3238; b) G. Zhou, W. Wong, *Chem. Soc. Rev.* **2011**, *40*, 2541–2566.
- [7] a) W. Sun, B. Zhang, Y. Li, T. M. Pritchett, Z. Li, J. E. Haley, *Chem. Mater.* **2010**, *22*, 6384–6392; b) T. M. Pritchett, W. Sun, B. Zhang, M. J. Ferry, Y. Li, J. E. Haley, D. Mackie, W. Shensky, A. G. Mott, *Opt. Lett.* **2010**, *35*, 1305–1307; c) Z. Li, E. Badaeva, D. Zhou, J. Bjorgaard, K. D. Glusac, S. Killina, W. Sun, *J. Phys. Chem. A* **2012**, *116*, 4878–4889; d) R. Liu, D. Zhou, A. Azenkeng, Z. Li, Y. Li, K. D. Glusac, W. Sun, *Chem. Eur. J.* **2012**, *18*, 11440–11448.
- [8] a) F. Guo, W. Sun, *J. Phys. Chem. B* **2006**, *110*, 15029–15036; b) F. Guo, W. Sun, *Inorg. Chem.* **2005**, *44*, 4055–4065; c) Z. Ji, Y. Li, T. M. Pritchett, N. S. Makarov, J. E. Haley, Z. Li, M. Drobizhev, A. Rebane, W. Sun, *Chem. Eur. J.* **2011**, *17*, 2479–2491; d) P. Shao, Y. Li, W. Sun, *Organometallics* **2008**, *27*, 2743–2749; e) Z. Ji, Y. Li, W. Sun, *Inorg. Chem.* **2008**, *47*, 7599–7607.
- [9] a) R. Liu, Y. Li, Y. Li, H. Zhu, W. Sun, *J. Phys. Chem. A* **2010**, *114*, 12639–12645; b) J. Yi, B. Zhang, P. Shao, Y. Li, W. Sun, *J. Phys. Chem. A* **2010**, *114*, 7055–7062; c) P. Shao, Y. Li, A. Azenkeng, M. R. Hoffmann, W. Sun, *Inorg. Chem.* **2009**, *48*, 2407–2419; d) B. Zhang, Y. Li, R. Liu, T. M. Pritchett, A. Azenkeng, A. Ugrinov, J. E. Haley, Z. Li, M. R. Hoffmann, W. Sun, *Chem. Eur. J.* **2012**, *18*, 4593–4606; e) P. Shao, Y. Li, T. M. Pritchett, W. Sun, *Inorg. Chem.* **2010**, *49*, 4507–4517; f) P. Shao, Y. Li, W. Sun, *J. Phys. Chem. A* **2008**, *112*, 1172–1179.
- [10] a) J. Schnelder, P. Du, X. Wang, W. W. Brennessel, R. Eisenberg, *Inorg. Chem.* **2009**, *48*, 1498–1506; b) D. Ravindranathan, D. A. K. Vezzu, L. Bartolotti, P. D. Boyle, S. Huo, *Inorg. Chem.* **2010**, *49*, 8922–8928; c) J. Schnelder, P. Du, P. Jarosz, T. Lazarides, X. Wang, W. Brennessel, R. Eisenberg, *Inorg. Chem.* **2009**, *48*, 4306–4316; d) S. Lai, H. Lam, W. Lu, K. Cheung, C. Che, *Organometallics* **2002**, *21*, 226–234.
- [11] a) G. S. Tong, C. Che, *Chem. Eur. J.* **2009**, *15*, 7225; b) S. C. F. Kui, I. H. T. Sham, C. C. C. Cheung, C. Ma, B. Yan, N. Zhu, C. Che, W. Fu, *Chem. Eur. J.* **2007**, *13*, 417; c) M. Yuen, S. C. F. Kui, K. Low, C. Kwok, S. S. Chui, C. Ma, N. Zhu, C. Che, *Chem. Eur. J.* **2010**, *16*, 14131–14141.
- [12] X. Liu, W. Sun, *Inorg. Chim. Acta* **2012**, *388*, 140–147.
- [13] H. F. Oehlschlaeger, I. R. MacGregor, *J. Am. Chem. Soc.* **1949**, *71*, 3223–3225.
- [14] S. Yao, K. J. Schafer-Hales, K. D. Belfield, *Org. Lett.* **2007**, *9*, 5645–5648.
- [15] K. D. Belfield, K. J. Schafer, W. Mourad, B. A. Reinhardt, *J. Org. Chem.* **2000**, *65*, 4475–4481.
- [16] C. E. Whittle, J. A. Weinstein, M. W. George, K. S. Schanze, *Inorg. Chem.* **2001**, *40*, 4053–4062.
- [17] Z. Ji, A. Azenkeng, M. Hoffmann, W. Sun, *Dalton Trans.* **2009**, 7725–7733.
- [18] S. Lai, M. C. W. Chan, K. Cheung, C. Che, *Inorg. Chem.* **1999**, *38*, 4262–4267.
- [19] a) D. J. Harter, M. L. Shand, Y. B. Band, *J. Appl. Phys.* **1984**, *56*, 865–868; b) Y. B. Band, D. J. Harter, R. Bavli, *Chem. Phys. Lett.* **1986**, *126*, 280–284; c) J. A. Hermann, J. Staromlynska, *Int. J. Nonlin. Opt. Phys.* **1993**, *2*, 271.
- [20] Y. Li, R. Liu, E. Badaeva, S. Kilina, W. Sun, *J. Phys. Chem. C* **2013**, *117*, 5908–5918.
- [21] E. C. Riesgo, X. Jin, R. P. Thummel, *J. Org. Chem.* **1996**, *61*, 3017–3022.
- [22] Y. Hu, M. Wilson, R. Zong, C. Bonnefous, D. R. McMillin, R. P. Thummel, *Dalton Trans.* **2005**, 354–358.
- [23] J. N. Demas, G. A. Crosby, *J. Phys. Chem.* **1971**, *75*, 991–1024.
- [24] J. Van Houten, R. J. Watts, *J. Am. Chem. Soc.* **1976**, *98*, 4853–4858.
- [25] I. Carmichael, G. L. Hug, *J. Phys. Chem. Ref. Data* **1986**, *15*, 1–250.
- [26] a) R. Bensasson, C. R. Goldschmidt, E. J. Land, T. G. Truscott, *Photochem. Photobiol.* **1978**, *28*, 277–281; b) S. Foley, G. Jones, R. Liuzzi, D. J. McGarvey, M. H. Perry, T. G. Truscott, *J. Chem. Soc. Perkin Trans. 2* **1997**, 1725–1730; c) C. V. Kumar, L. Qin, P. K. Das, *J. Chem. Soc. Faraday Trans.* **1984**, *280*, 783–793.
- [27] P. A. Firey, W. E. Ford, J. R. Sounik, M. E. Kenney, M. A. J. Rodgers, *J. Am. Chem. Soc.* **1988**, *110*, 7626–7630.
- [28] W. Sun, H. Zhu, P. M. Barron, *Chem. Mater.* **2006**, *18*, 2602–2610.

Received: April 10, 2013
Published Online: July 9, 2013